

## Research Article

<https://doi.org/10.1631/jzus.A2300372>

# Chemical oxygen demand oxidation via sustained-release persulfate balls: a rate-compatibility study of flow velocity, releasing, and oxidation

Bate BATE<sup>1</sup>, Danting ZHANG<sup>2✉</sup>, Jianshe YE<sup>3</sup>, Min XIA<sup>4</sup>, Yixin YANG<sup>1</sup>, Shuai ZHANG<sup>1</sup>

<sup>1</sup>Institute of Geotechnical Engineering, Zhejiang University, Hangzhou 310058, China

<sup>2</sup>Shanghai Envirunion Eco-technology Co., Ltd, Shanghai 201106, China

<sup>3</sup>China Railway Eryuan Engineering Group East China Survey and Design Co., Ltd, Hangzhou 310000, China

<sup>4</sup>The Architectural Design & Research Institute of Zhejiang University Co., Ltd, Hangzhou 310027, China

**Abstract:** Chemical oxygen demand (COD) in municipal solid waste (MSW) landfill leachates is a challenging problem. This paper investigated the feasibility of using sodium persulfate (PS), a strong oxidant, as a permeable reactive barrier (PRB) filling material. Firstly, sustained-release persulfate balls were manufactured to adjust the release rate of persulfate, the oxidation agent. In addition, Fe(II) loaded activated carbon was used to help with an even distribution of Fe(II) in the porous medium (PRB in this case). Then, the oxidation efficiency and kinetic rate of COD removal by the sustained-release balls were subjected to batch tests. It was found that a ratio of 1:1.4:0.24:0.7 for sodium persulfate: cement: sand: water was the most efficient for COD removal (95%). From the breakthrough curve for a 5 mm sustained-release ball, it was found that the retardation factor was 1.27 and the hydrodynamic dispersion coefficient was 15.6 cm<sup>2</sup>/d. The corresponding half-life of COD oxidation was 0.43 d, which was comparable with the half-life of PS release from sustained-release balls (0.56 d). The sustained-release persulfate balls were shown to be an economical material with a simple recipe and production method when catalyzed by Fe-AC. Sustained-release balls used in PRBs offer significant advantages in terms of both effectiveness and economy compared with cutting-edge methods for the preparation of sustained-release and catalytic materials. These results verified the feasibility of sustained-release persulfate balls as a PRB material for COD removal.

**Keywords:** Chemical oxygen demand, sodium persulfate, sustained-release ball, permeable reactive barrier, Fe-AC


## 1 Introduction

MSW landfills are the most common type of sanitary landfills, both inside and outside downtown areas, and can pollute soil and groundwater with biodegradation products (Dumont et al., 2017). Among these are organic compounds, designated as COD, consisting primarily of humic acids and fulvic acids, which are difficult to remove by degradation

or oxidization (Ye et al., 2019). The concentration of COD can be as high as of the order of 10,000 mg/L in the leachate, yet it is often lowered to less than 500 mg/L near the MSW piles, a concentration range that can be cleaned by PRB (Han et al., 2016).

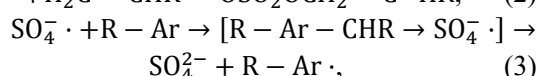
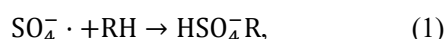
Compared to ammonium persulfate and potassium persulfate, sodium persulfate is stable and safe in terms of melting point, relative density, water solubility, pH, and half-lethal dose of acute poisoning. PS can be easily dissociated in water to release persulfate anions. It is also stable and requires certain conditions, such as heat, UV light, or the presence of transition metals (Tsitonaki et al., 2010; Li, 2018), to generate sulfate radical anions. These anions, given their high oxidation potential, can oxidize most organic contaminants mainly by

✉ Danting ZHANG, 785277034@qq.com

 Bate BATE, <https://orcid.org/0000-0002-8692-8402>

Danting ZHANG, <https://orcid.org/0009-0004-0360-8932>

three types of chemical reactions, namely: the detachment of hydrogen Eq. (1) for saturated organic compounds (alkanes, ethers, alcohols, esters); one-electron oxidation Eq. (2) for organic contaminants with benzene rings (benzodiazepines, aromatics); and the addition of multiple bonds Eq. (3) for unsaturated olefin and alkyne organic compounds (Neta. et al., 1977; Clifton and Huie, 1989; Padmaja et al., 1993; Khursan et al., 2006).



Certain metal ions, such as iron, can catalyze sodium persulfate and generate higher-oxidation state sulfate radicals for oxidizing organic compounds. When used as an activator for sodium persulfate in PRB, metal ions should be carried by porous media. Carbon-based materials, such as activated carbon fibers, multiwall carbon nanotubes, activated carbon, coal-based carbon membrane, and biochar, are commonly used as carriers in PRB due to their high chemical and physical activities, lack of secondary pollution, good biocompatibility, good acid and alkali resistance, and controllability (Table 1) (Feng et al., 2015; Li et al., 2016b; Zhang et al., 2016; Hussain et al., 2017; Wang, 2017; Song et al., 2018; Dong et al., 2019a; Lee et al., 2020; Ma et al.,

2023a; Ma et al., 2023b). Graphene and multiwall carbon nanotubes are less commonly used due to their high cost compared to activated carbon. Activated carbon is cheap with well-developed pore structure, high specific surface area and surface chemical groups (i.e., hydroxyl, carboxyl). It is environmentally friendly, strongly adsorptive to ions and easy to modify. Therefore, activated carbon has been widely used as a catalyzing agent carrier and high-capacity absorbent (Veerakumar et al., 2016; Kamaraj et al., 2020; Singh et al., 2023). Iron, an economical and abundant natural material, is often used as a cost-effective and environmentally friendly option for modifying activated carbon. It readily attaches to sodium persulfate-loaded activated carbon and serves not only as an absorbent material but also as a heterogeneous catalyst (Li, et al., 2016b; Lee, et al., 2020; Zhao et al., 2021; Zhao et al., 2023). Divalent iron fixation on granular activated carbon has been widely used in PRB (Goyal et al., 2023). Zhao, et al. (2021) found that Fe(II)-loaded activated carbon, as a catalyst material for the oxidant reaction, exhibited stability with low leakage of iron cations. Despite the fact that iron-loaded activated carbon can catalyze sodium persulfate to oxidize organic compounds effectively (Li et al., 2016a; Kalaruban et al., 2019), to date its oxidation capacity on organic compounds (COD) from MSW pile leachates has not been reported.

**Table 1 Catalyst types of persulfate**

Catalyst	Contamination	Reference
N-doped coal-based carbon membrane	Bisphenol A(BPA)	Ma, et al. (2023a)
Fe <sub>3</sub> O <sub>4</sub> /multi-walled carbon nanotubes	Flumequine	Feng, et al. (2015)
Fe <sub>2</sub> O <sub>3</sub> nanoparticle/oxidize carbon nanotube membrane	Tetracycline(TCE)	Ma, et al. (2023b)
CuFe <sub>2</sub> O <sub>4</sub> /Activated carbon	Coking wastewater	Song, et al. (2018)
CuFe <sub>2</sub> O <sub>4</sub> /multi-walled carbon nanotubes	Diethyl phthalate (DEP)	Zhang, et al. (2016)
nZVI/Rice husk biochar	Phthalate	Dong et al. (2019b)
nZVI/Biochar	Nonyl phenol	Hussain, et al. (2017)
Fe <sup>2+</sup> /Activated carbon	Perfluorooctanoic acid	Lee, et al. (2020)
Fe <sup>2+</sup> /Activated carbon	Landfill leachate (COD)	Li, et al. (2016b)
Iron-based sludge biochar	Organic wastewater	Wang (2017)

Following a comparison of methods for preparing sustained-release materials, such as coating, freeze-thaw, sol-gel, oil-phase separation,

and mixing with binders, a cost-effective, time-efficient, and user-friendly approach was chosen (Kang et al., 2004; Lee and Schwartz, 2007; Liang

et al., 2011; Lin et al., 2012; Rauscher et al., 2012; Chen et al., 2013; Lee and Gupta, 2014; Sakulthaew and Chokejaroenrat, 2016; Yang et al., 2016; Omoike and Harmon, 2019; Wang et al., 2023). As found by Wang, et al. (2023), the release of sodium persulfate from pellets fits a second-order kinetics equation. However, the reaction is affected by the large area of pores and cracks. This method entails mixing cement, sand, and water with oxidizing agents, such as sodium persulfate, to produce sustained-release sodium persulfate balls with a mass ratio of 1:1.4:0.24:0.7 for sodium persulfate, cement, sand, and water. Sustained-release balls with a certain ratio of sodium persulfate ensured a continuous release of the oxidizing agent ( $S_2O_8^{2-}$ ) (Liang, et al., 2011). The price of sustained-release persulfate balls was calculated to be 3.3 RMB per kilogram.

In PRB engineering, the sustained release of sodium persulfate is needed. However, sodium persulfate has a short half-life and cannot be used directly as a PRB filling material (Lee, et al., 2020; Zhao, et al., 2021; Zhao, et al., 2023). The selection of filling materials for PRBs should consider the potential formation of precipitates, as they can lead to barrier clogging, reducing both permeability and overall effectiveness (Budania and Dangayach, 2023). In addition, the temporospatial heterogeneity of persulfate oxidation due to preferential flow in PRB can generate pore-blocking precipitates and by-pass flow, which make contaminants in low-permeable zones difficult to degrade (Ross et al., 2005). To tackle the above problems, processed sustained-release balls of sodium persulfate were manufactured to control the release rate of PS and enhance its lifetime. At present, no quantitative study is available on the release time of sustained-release PS balls or their compatibility with the oxidation time for COD removal.

The goal of this study was to explore the feasibility of implementing sodium persulfate sustained-release balls in a PRB and to obtain the matched chemical kinetics for the sustained release of PS and the COD oxidation reaction by optimizing the ball size.

## 2 Materials and Experimental Methods

### 2.1 Materials

The particle size of activated carbon used in this study ranged from 1 to 2 mm (Shanghai Xinhui Activated Carbon Co., Ltd). The cement was PI 42.5 Portland cement (China General Academy of Building Materials Science Research Co., Ltd). Analytical reagent potassium hydrogen phthalate ( $C_8H_5KO_4$ ), sodium persulfate ( $Na_2S_2O_8$ ), iron vitriol ( $FeSO_4 \cdot 7H_2O$ ), potassium dichromate ( $K_2Cr_2O_7$ ), sulfuric acid ( $H_2SO_4$ ), silver sulfate ( $Ag_2SO_4$ ), mercury sulfate ( $HgSO_4$ ), potassium iodide (KI), and sodium bicarbonate ( $NaHCO_3$ ) were used in this study. Contaminated leachate samples were collected from Hangzhou Tianziling Landfill and were stored in a freezer before testing. The COD concentration of the leachate was determined to be 778 mg/L.

Fe(II)-loaded activated carbon (Fe(II)-loaded AC) with grain sizes of 1 to 2 mm was produced as follows: activated carbon was soaked in 1% sulfuric acid overnight, rinsed with deionized water, and oven-dried for 24 h at 105°C. Ten grams of oven-dried activated carbon were mixed with 50 mL of 0.1 mol/L iron vitriol solution in a thermostatic oscillator for one hour to load divalent iron on the activated carbon surface. The resulting Fe(II)-loaded AC was oven-dried for 2 hours at 65°C, then calcined in a tubular furnace at 550°C under nitrogen to oxidize the divalent iron (Li, 2016). The Fe(II)-loaded AC was stored in a vacuum dryer before use.

The sustained-release sodium persulfate balls with a grain size ranging from 5 to 20 mm were manufactured by Zhejiang University. Ottawa sand with a diameter range of 20 to 30 mesh and the cement were manufactured by China General Academy of Building Materials Science Research Co., Ltd. Sodium persulfate, cement, sand, and water were prepared with the ratio mentioned above. In a 500 mL beaker, sodium persulfate, cement, and sand were added, followed by the addition of water. The components were continuously mixed for 15-20 minutes. The resulting pasty liquid was poured into molds with diameters ranging from 5 to 20 mm and air-dried for 1 day at room temperature (25°C) to fix the shape (Liang, et al., 2011).

### 2.2 Experimental Methods

#### 2.2.1 Microscopic Characterization

Nitrogen adsorption tests on unmodified activated carbon and Fe(II)-loaded AC samples were performed by a fully automatic specific surface and micropore size analyzer to measure the specific surface area, total pore volume, and pore distribution. For the pore throat structure, Micrometrics AutoPore IV 9500 Mercury Intrusion Porosimetry (MIP) was used at a pressure of 206.844 MPa in the test.

Unmodified and Fe(II)-loaded AC samples were tested with topography and elemental analysis using scanning electron microscopy (SEM) and electron energy dispersive spectroscopy (EDS).

Fe(II)-loaded or unloaded activated carbon samples were taken for mineral composition and functional group tests using X-ray diffraction (XRD) and Fourier transform infrared spectroscopy (FTIR) methods. XRD was performed using an Advance D8A25 powder X-ray diffractometer (Bruker, Germany), data was analyzed using software MDI Jade 6 (v.6.5.26; *Material Data, Inc.*, CA, USA) and a NicoLeT iS50FT-IR (Thermo Scientific, USA) for FTIR method with a resolution range of  $400\text{ cm}^{-1}$  and  $4000\text{ cm}^{-1}$  collected 32 scans with a KBr of  $4\text{ cm}^{-1}$ .

### 2.2.2 Chemical Concentrations

To determine the COD removal efficiencies by PS oxidation, batch tests were performed according to the following steps: (1) 100 mL of contaminated solution was diluted twice, 0.278 g of iron vitriol, and PS (0.119 g, 0.238 g, 0.476 g, 1.19 g) were placed in a 250 mL conical flask. (2) 100 mL of contaminated solution was diluted twice, PS (0 g, 0.119 g, 0.238 g) and 1 g of unloaded Fe(II)-loaded AC was placed in a 250 mL conical flask. (3) 100 mL of contaminated solution was diluted twice, PS (0.5 g, 0.238 g, 0.476 g), and 1 g Fe(II)-loaded AC was placed in a 250 mL conical flask. The conical flasks were put in a thermostatic oscillator at a temperature of  $20^\circ\text{C}$  and 150 r/min rotation speed, then 1 mL of sample was taken at time stamps of 20 mins, 40 mins, 60 mins, 80 mins, 100 mins, and 120 mins for COD concentration tests. The sample collection method was following the aquarium leaching test (EU standard NEN 7375), which was carried out to obtain the release rate of cement sustained-release balls (Kosson et al., 1996; Chen, et

al., 2013). In the leaching experiment, sustained-release sodium persulfate balls with particle sizes ranging from 5 to 20 mm with 100 mL deionized water were placed in 250 mL conical flasks, the leaching solution was replaced, and samples were taken according to a timetable at 0.25, 1, 2.25, 4, 9, 16, 32, and 64 days. The concentration of sodium ions was obtained using an S23A visible light spectrophotometer (Shanghai Lengguang Technology Co., Ltd) at 352 nm to estimate the cumulative release volume and release rate of sodium persulfate according to Eq. (4).

$$q = \frac{CV}{M}, \quad (4)$$

where  $q$  is the cumulative release volume (mg/g);  $C$  is the concentration of sodium ions;  $V$  is the volume of deionized water; and  $M$  is the mass of sustained-release sodium persulfate ball.

In order to obtain the release rate of sustained-release sodium persulfate balls, a batch test was carried out as follows: the 100 mL twice-diluted contaminated solution was placed in 250 mL conical flasks, together with 1 g of Fe(II)-loaded AC and two or four pebbles of sustained-release sodium persulfate balls, which contained either 1 or 2 mmol sodium persulfate. The flasks were placed in a thermostatic oscillator with 150 r/min rotation speed at  $20^\circ\text{C}$ . One mL sample was obtained for COD concentration measurement, at time steps of 20, 40, 60, 80, and 100 minutes, as well as 2, 4, 6, 24, and 48 hours.

Inductively coupled plasma-mass spectrometry (ICP-MS) (ICAPRQICPMS, Thermo Fisher Scientific, USA) was used for the iron concentration test.

Rapid-resolution spectrophotometry tests were performed for the COD concentration measurement. One mL  $0.24\text{ mg/L Ag}_2\text{SO}_4$  and  $0.5\text{ mol/L K}_2\text{Cr}_2\text{O}_7$  ( $\text{Ag}_2\text{SO}_4:\text{K}_2\text{Cr}_2\text{O}_7=1:2$ ) solution, with 4 mL  $10\text{ g/L}$  sulfuric acid-silver sulfate solution was placed in a Hash digestion tube, shaken well, added to 2 mL of samples and digested for 15 min at  $165^\circ\text{C}$  in the digester. The absorbance was measured after cooling at 440 nm for the concentration range between 15-250 mg/L, and at 600 nm for the concentration range between 100-1000 mg/L.

The persulfate concentration test was determined spectrophotometrically using the iodometry method. Firstly, a  $0.2\text{ mmol/L}$  sodium

persulfate stock solution was prepared. Then, 0.00, 2.00, 4.00, 6.00, 10.00 and 12.00 mL stock solutions were separately pipetted into 50 mL test tubes and were diluted with deionized water. Thirdly, 0.2 g of sodium hydrogen carbonate and 4 g of potassium iodide were added, diluted to 50 mL with deionized water and shaken for the full-color reaction. The relation between absorbance at 352 nm and persulfate concentration showed high linearity with  $R^2=0.991$  as illustrated in Fig. 1 (Guo, 2013). The equation ( $y = 0.0475x - 0.0038$ ) can be applied to calculate the sodium persulfate residue in the kinetic experiment of the COD oxidation reaction, enabling the determination of COD concentrations.

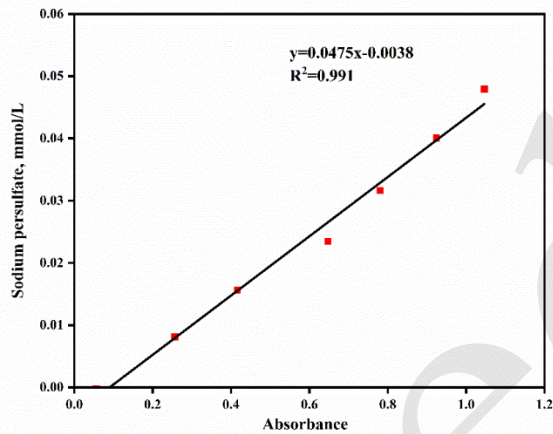


**Fig. 1 Relationship between sodium persulfate and absorbance**

### 2.2.3 Preparation Method for PS Sustained-Release Balls

The mass ratio of sodium persulfate: cement: sand: water mass ratio was set as 1:1.4:0.24:0.7, which was the ratio used by Liang, et al. (2011). Sand content was the dominant factor for the sustained release of PS at sand: cement ratios over 1, as opposed to a cement-dominant ratio, i.e., sand: cement ratio less than 1.

The breakthrough test was performed in a plexiglass column (Fig. 2) with a length of 50 cm and a diameter of 5 cm. The filler materials, from bottom to top, were Ottawa sand (15 cm), sustained-release sodium persulfate balls (5 cm; approximately 380 pebbles), Ottawa sand (10 cm),

Fe(II)-loaded AC (5 cm), Ottawa sand (5 cm), activated carbon (5 cm), and Ottawa sand (5 cm). There were three sample collection holes on the sidewall at distances of 20, 35, and 50 cm from the column base. The inflow solution, with a diluted COD concentration of 200 mg/L and pH of 7.1, was peristaltically pumped from the column base at a flow rate of 0.3 mL/min. Effluent samples were collected at the specified intervals and stored in a dark environment for COD concentration measurement. The ambient temperature was 15°C.

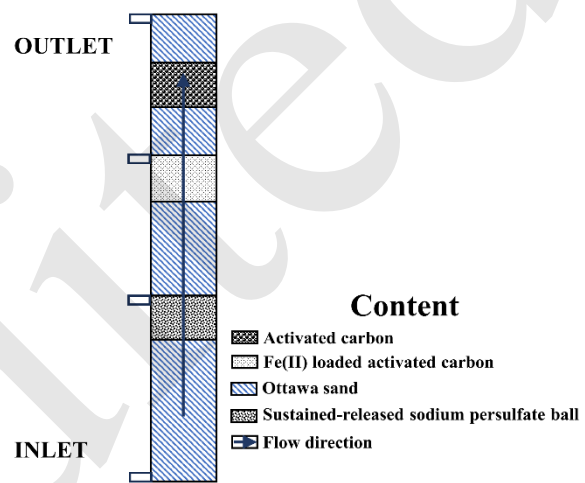


**Fig. 2 Break-through column test setup**

**Table 2 Properties of the PRB filler materials**

Filling materials (from bottom to top)	Filling thickness (cm)	Filling mass (g)
Ottawa sand	15	493
Sustained-release sodium persulfate ball	5	122
Ottawa sand	10	388
Fe(II)-loaded AC	5	62
Ottawa sand	5	185
Activated carbon	5	61
Ottawa sand	5	181

## 3 Results

### 3.1 Microscopic characteristics

Compared with unloaded AC, the specific

surface area of Fe(II)-loaded AC decreased by 25% (from 1143.56 to 867.37 m<sup>2</sup>/g). A significant decrement in microporous pore volume (Fig. 3a) was also observed after Fe(II) loading, probably due to the crystals of Fe(II) occupying and clogging the

micropores of AC (Kalaruban, et al., 2019). This is supported by the decrease in the micropore radius from 1.91 nm to 1.90 nm according to the BET result and the reduction in diameter from 1.61 μm to 1.31 μm based on the MIP result (Fig. 3).

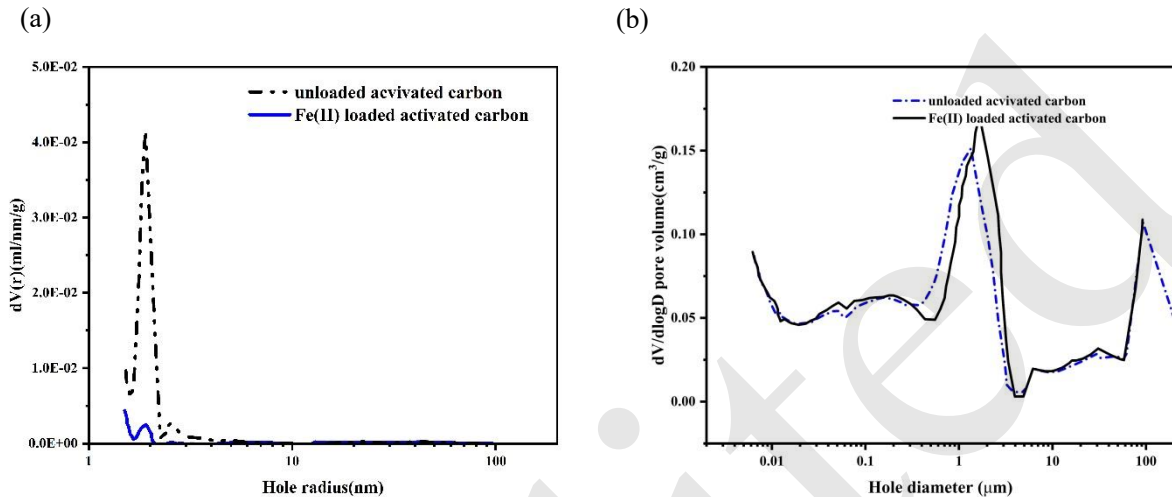


Fig. 3 Pore distribution of activated carbon before and after iron loading using (a) BJH and (b) MIP methods.

According to the SEM and EDS results of Fe(II)-loaded or unloaded AC, the surface of activated AC contained large amounts of small openings (Fig. 4a). The surface of Fe(II)-loaded AC contained iron aggregates (Fig. 4b). Sodium persulfate grains with particle sizes between 170 and 200 μm were uniformly distributed in the

sustained-release balls (Fig. 5). From the EDS of the SEM images (Fig. 7), the primary elements of the sustained-release ball were Ca and Si, which agrees with the chemical compositions of cement (CaO and SiO<sub>2</sub>) and sodium persulfate insertion (Na and S).

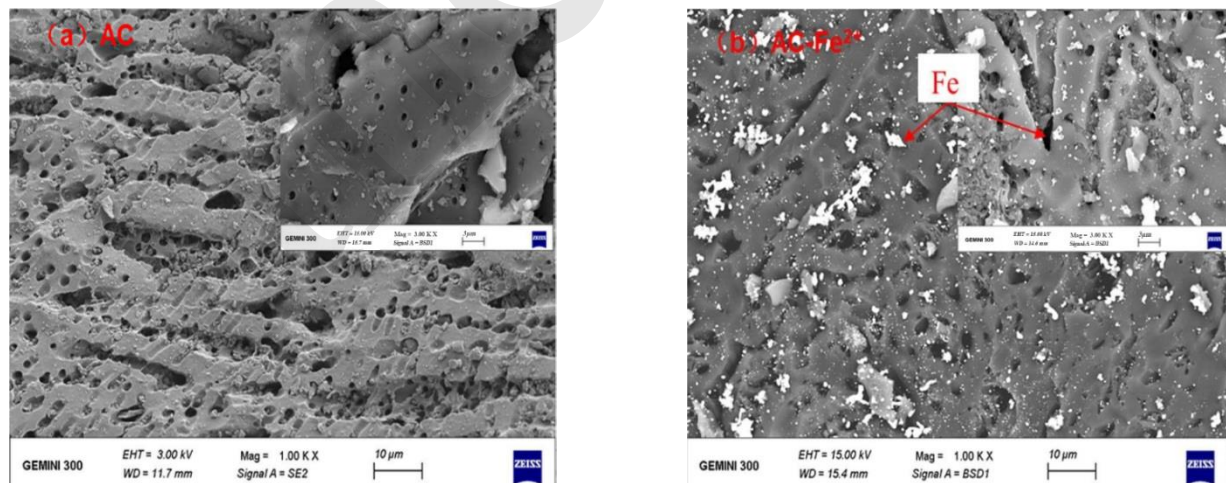


Fig. 4 SEM of activated carbon before and after Fe loading

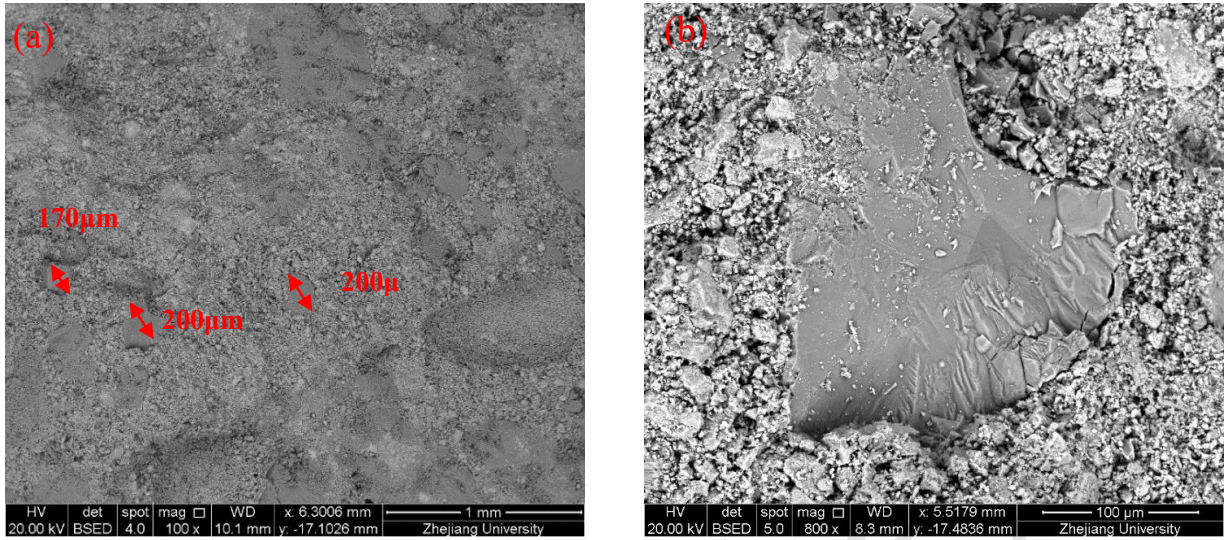


Fig. 5 SEM of sustained-release sodium persulfate ball

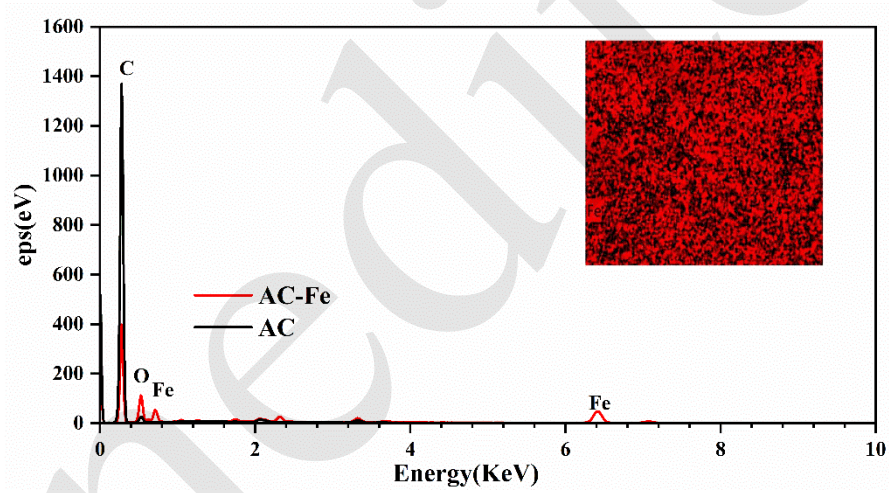
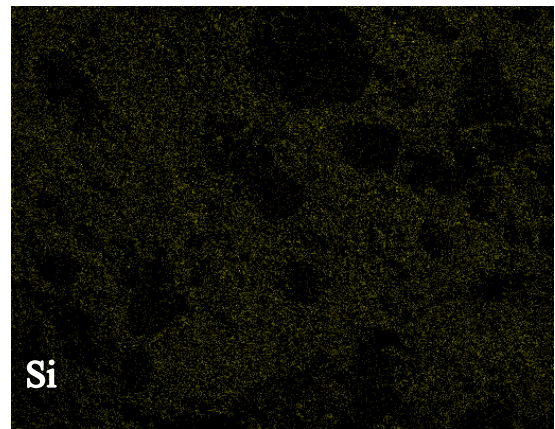
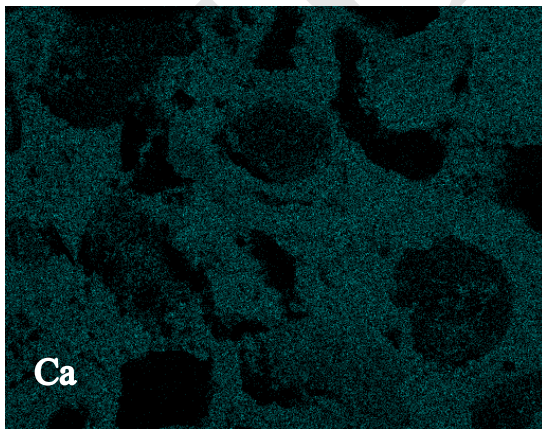


Fig. 6 EDS of activated carbon before and after Fe loading



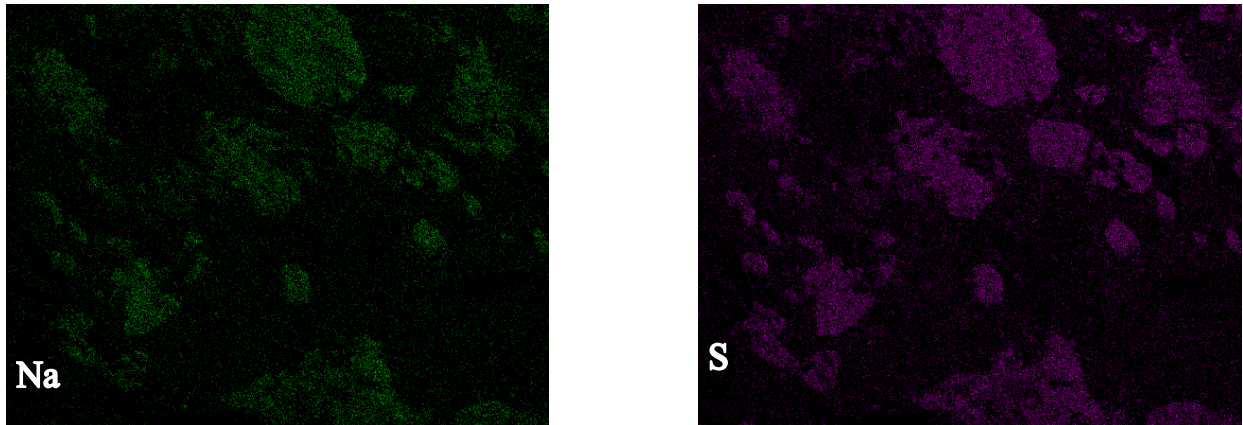


Fig. 7 EDS of sustained-release sodium persulfate ball

According to the XRD results, unloaded AC consisted primarily of carbon; while after the loading of the ferro-compound, new minerals, mainly ferric oxide ( $\text{Fe}_2\text{O}_3$ ) and ferric oxide ( $\text{Fe}_3\text{O}_4$ ), were identified using software MDI Jade 6.

From the FTIR results, the characteristic peaks of activated carbon at  $3431\text{ cm}^{-1}$ ,  $1560\text{ cm}^{-1}$ ,  $1384\text{ cm}^{-1}$ , and  $1109\text{ cm}^{-1}$  were O-H stretching vibration (Abdullah et al., 2018; Zhang et al., 2018), C=C bending vibration (Barroso-Bogeat et al., 2019),  $\text{CH}_3$  attributed vibration (Das et al., 2008), and C-O stretching vibration (Cheng et al., 2016; Zhang, et al., 2018), respectively. The Fe-O stretching vibration appeared with a band at  $700\text{--}500\text{ cm}^{-1}$  (Krishnan and Haridas, 2008) and the Fe-O-H stretching vibration appeared with a band at  $700\text{--}500\text{ cm}^{-1}$  (Mehrabi et al., 2015). The characteristic peaks of Fe(II)-loaded AC were changed from  $3431\text{ cm}^{-1}$  to  $3434\text{ cm}^{-1}$ , from  $1560\text{ cm}^{-1}$  to  $1572\text{ cm}^{-1}$ , and from  $1109\text{ cm}^{-1}$  to  $1120\text{ cm}^{-1}$ , suggesting that the intensity of Fe(II)-loaded AC was higher than unloaded AC due to the accumulation of iron contained in those functional groups. This indicates that iron was effectively loaded on the surface of the activated carbon (Mehrabi, et al., 2015).

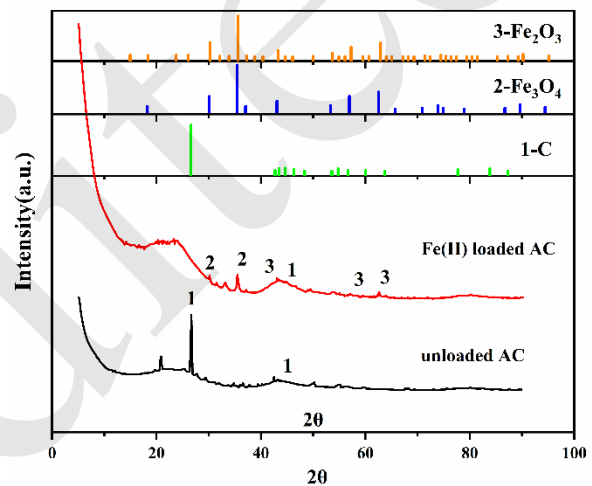


Fig. 8 XRD of activated carbon before and after Fe loading

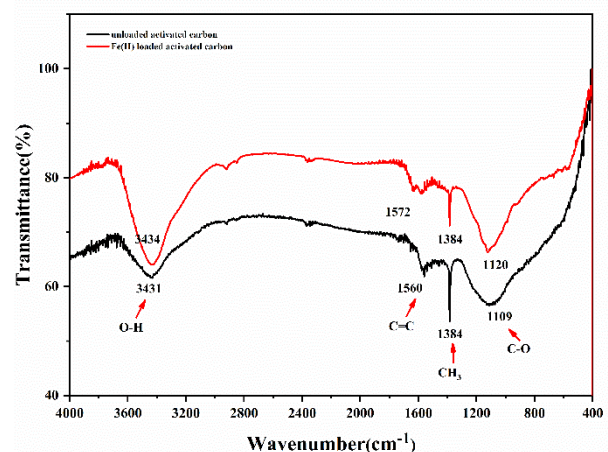


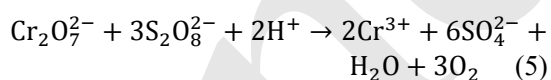
Fig. 9 FTIR of activated carbon before and after Fe loading



Based on the above results, it is postulated that the unique structure of Fe(II)-loaded AC enhances its chemical activity based on three mechanisms: (1) Large specific surface area and micropores increase the number of reaction sites for the absorbance of contaminants in the catalytic reaction. (2) The carbon of Fe(II)-loaded AC contains a high  $sp^2$  hybrid carbon ratio, which is more conducive to the radioactivation of sodium persulfate based on the high defect density (Tian et al., 2018). (3) Enhancement in the electronic conductivity and facilitated electronic transfer capability enables the graphitization of the Fe(II)-loaded AC, as shown by the XRD result, where a  $43.3^\circ$  diffraction peak emerged ( $2\theta$ ), a typical characteristic of graphitization (Gong et al., 2017). (4) Fe(II)-loaded AC reduces the local functional groups of the carbon surface and improves interfacial electron transfer (Yao et al., 2016). (5) Carbon coatings can prevent iron ions from rapid corrosion (Lee, et al., 2020).

### 3.2 Kinetics of the COD oxidation reaction

It has been reported that sodium persulfate could be misidentified as the result of COD in rapid-resolution spectrophotometry, which overestimates the actual COD. The chemical reaction equation involved is as follows (Zeng et al., 2017):



Based on Eq. (5), the relationship between sodium persulfate and the falsely identified COD concentration, namely, 1 g/L PS equals 66.88 mg/L of COD, was calibrated (Fig. 10).

Then, the actual COD concentration was obtained by subtracting the residue of sodium persulfate in the sample from the measured COD concentration (Wang et al., 2014; Yang, 2016). Applying the first-order kinetics reaction assumption to the COD removal by Fe-AC catalyzing sodium persulfate, the fitted constant of reaction rate  $K$  is  $0.83 \text{ hr}^{-1}$  and the half-life period  $t_{0.5}$  is 0.83 hrs.

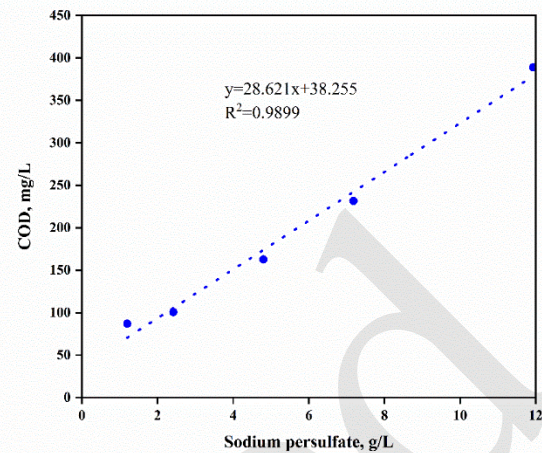


Fig. 10 Relationship between sodium persulfate and COD identified by rapid resolution spectrophotometry

Applying the pseudo-first-order kinetics reaction assumptions (Fig. 11) to the COD removal by four pebbles of sustained-release sodium persulfate balls catalyzed with Fe(II)-loaded AC, yielded a fitted constant of reaction rate ( $K$ ) of  $0.15 \text{ hr}^{-1}$  and a half-life period ( $t_{0.5}$ ) of 4.62 hrs.

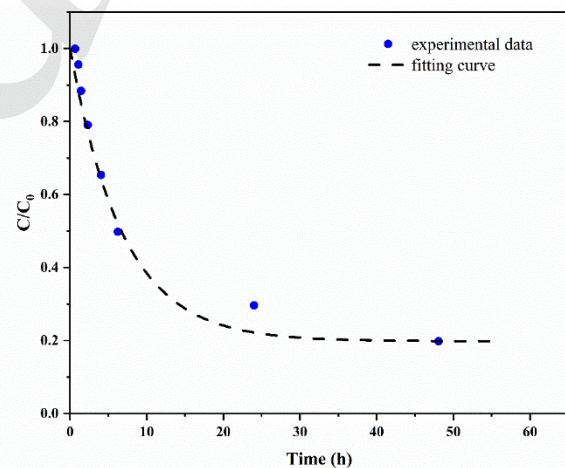


Fig. 11 AC/Fe-PPS2 (Fe(II)-loaded AC and four pebbles sustained-release sodium persulfate balls containing 2 mmol sodium persulfate) pseudo-first-order kinetics fitting curve

### 3.3 COD Removal Efficiency

As the PS: Fe ratio was increased from 0.5:1 to 1:1 and 2:1, the removal rate of COD increased from 68% to 80% and 95%, respectively. By Fe(II) activation, the higher ratio of PS led to the

production of more sulfate radicals, which in turn oxidized more COD in the fluid. Further increment of PS content, at a PS: Fe ratio of 5, led to a drastic decrease in COD removal rate (33%) Given the high activity of sulfate radicals, their abundance in the fluid could be wrongly identified as COD (elaborated in the preceding paragraph), which could yield a low COD removal rate. On the other hand, it should be noted that at a low PS content

(PS: Fe(II)) ratio of 0.5,  $\text{Fe}^{2+}$  consumes sulfate radicals ( $\text{SO}_4^{\cdot -}$ ), leading to a low COD removal rate (68%) Eq. (6). Furthermore, divalent  $\text{Fe}^{2+}$  in the solution form is easily oxidized by oxygen in the air. Therefore, direct addition of  $\text{Fe}^{2+}$  into the PRB is not practical. Alternatively, Fe(II) loaded onto AC (Fe-AC) is stable and applicable to PRB. Its effects on COD removal will be elaborated on later.

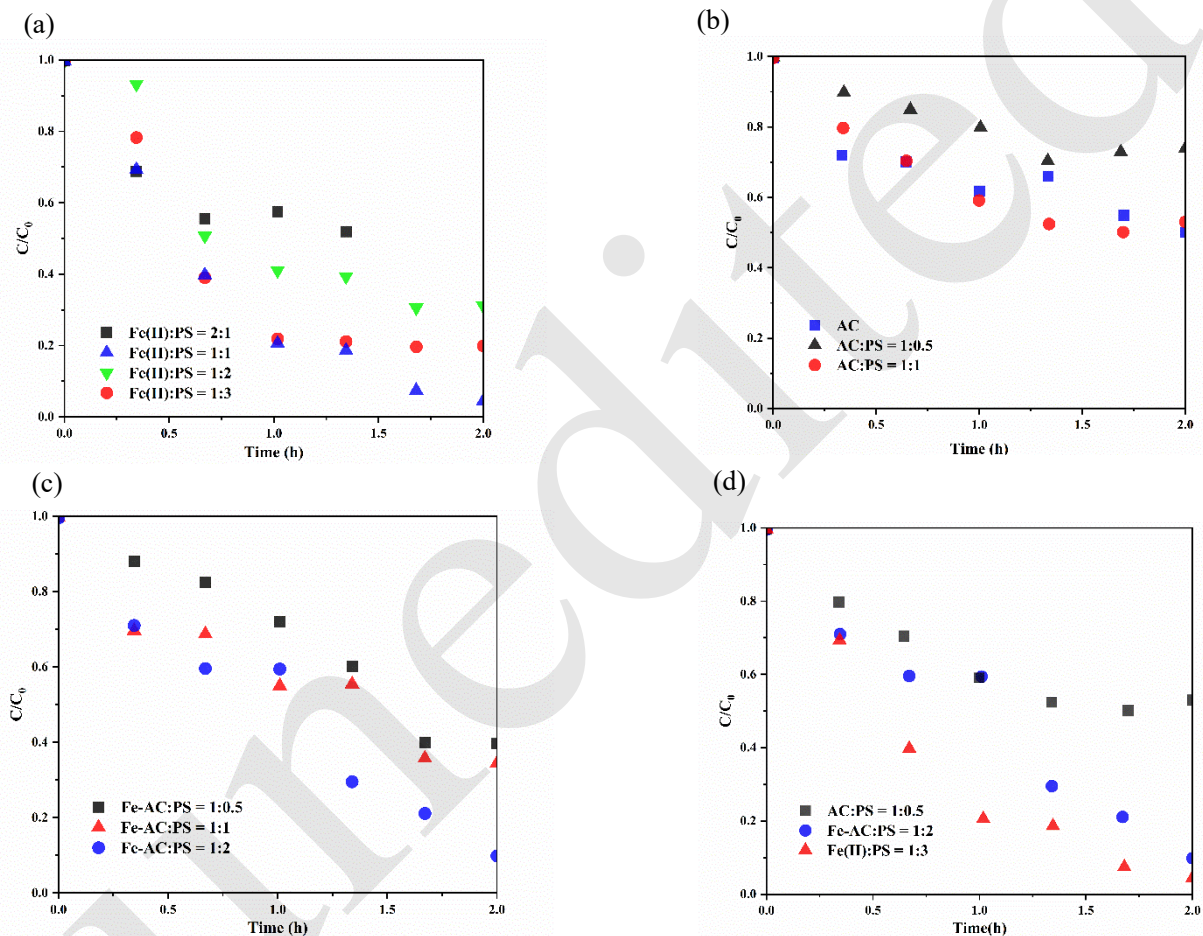
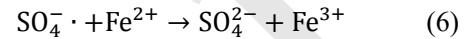


**Fig. 12** Time-evolution curves of normalized COD concentration by (a) PS and Fe(II) (sodium persulfate and ferrous sulfate in a certain ratio), (b) PS and AC (sodium persulfate and activated carbon in a certain ratio), and (c) PS and Fe(II)-loaded AC (sodium persulfate and Fe(II)-loaded activated carbon in different ratios), (d) PS and Fe(II), PS and AC as well as PS and Fe(II)-loaded AC with sodium persulfate

The COD removal rates via both AC and alone were below 27% (Fig. 12(a)). Activated carbon can absorb COD, and the hydroxy and carboxyl groups on activated carbon can further catalyze sodium persulfate to generate sulfate radicals to oxidize COD (Xu et al., 2012), which improves the COD

removal rates by up to 58% with AC: PS ratios of 1.

Given 1 g of Fe-AC, the COD removal rate increased from 62% to 67% and to 90% as the PS content increased from 0.119 g to 0.238 g and then to 0.476 g. At a 90% COD removal rate, the concentrations of  $\text{S}_2\text{O}_8^{2-}$  and  $\text{Fe}^{2+}$  were 4.76 g/L and

8.5 g/L, respectively, and the  $S_2O_8^{2-}$ :12COD ratio was 1.02. The catalysis of sodium persulfate by Fe-AC resulted in an impressive COD removal rate of up to 90%, while also mitigating the disadvantage of  $Fe^{2+}$  easily oxidizing in the presence of air. From the above measurements, the fitted chemical kinetic constants can be determined: the kinetic rate constant ( $K$ ) at  $0.83\text{ h}^{-1}$  and the half-time ( $t_{0.5}$ ) at 0.83 hrs.

### 3.5 Release rate of sustained-release sodium persulfate balls

The released cumulative sodium persulfate for 4 particle diameters fitted well with the hyperbolic kinetics models, and the relationship between the

released cumulative PS amount  $q$  (mg/g) and time is:

$$\frac{1}{q} - \frac{1}{q_{\max}} = \frac{1}{kt} \tag{7}$$

Eq. (7) can be converted to Eq. (8) to Eq. (10), so that

$$q = q_{\max} \left( 1 - \frac{1}{1 + \frac{kt}{q_{\max}}} \right) \tag{8}$$

$$t = \frac{q_{\max}}{k} \frac{a}{1-a} \tag{9}$$

$$t_{0.5} = \frac{q_{\max}}{K} \tag{10}$$

where  $q_{\max}$  is the maximum released amount of the sustained-release sodium persulfate ball, mg/g;  $K$  is the rate of release, mg/g/d;  $a = \frac{q}{q_{\max}}$  - release;  $t_{0.5}$  is the half-life (PS release of 50%). The fitting parameters are listed in Table 5.

**Table 3 Release rate of sustained-release sodium persulfate balls**

Particle size (mm)	Fitting curve	Release rate (mg·(g·d) <sup>-1</sup> )	$t_{0.5}$ (d)
5	$q_1 = 7098t / (63.14 + 112.27t)$	112.27	0.56
10	$q_2 = 4370t / (55.23 + 79.14t)$	79.14	0.70
15	$q_3 = 1064t / (35.92 + 29.60t)$	29.6	1.21
20	$q_4 = 778t / (32.91 + 23.63t)$	23.63	1.39

A linear relationship ( $R^2=0.945$ ) between the ball diameter and half-life was observed:

$$t_{0.5} = 0.060d + 0.215 \tag{11}$$

The ball diameter and kinetic rate constant of PS release ( $K$ ) were inversely proportional:

$$y = 544.6/d \quad (R^2=0.8591) \tag{12}$$

**Table 4 Sustained-release ball parameters with different sizes**

Particle size (mm)	$q_{\max}$ (mg/g)	$K$ (mg/g/d)	SSE	$R^2$
5	63.14	112.27	14.61	0.9879
10	55.23	79.14	16.77	0.9873
15	35.92	29.60	15.82	0.9779
20	32.91	23.63	8.05	0.9872

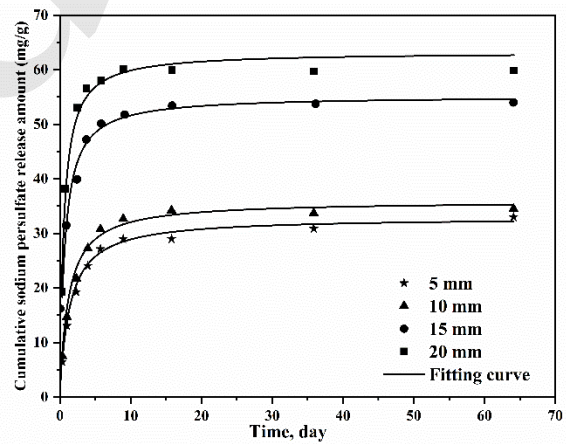


**Fig. 13 PS cumulative release amount and fitting curve**

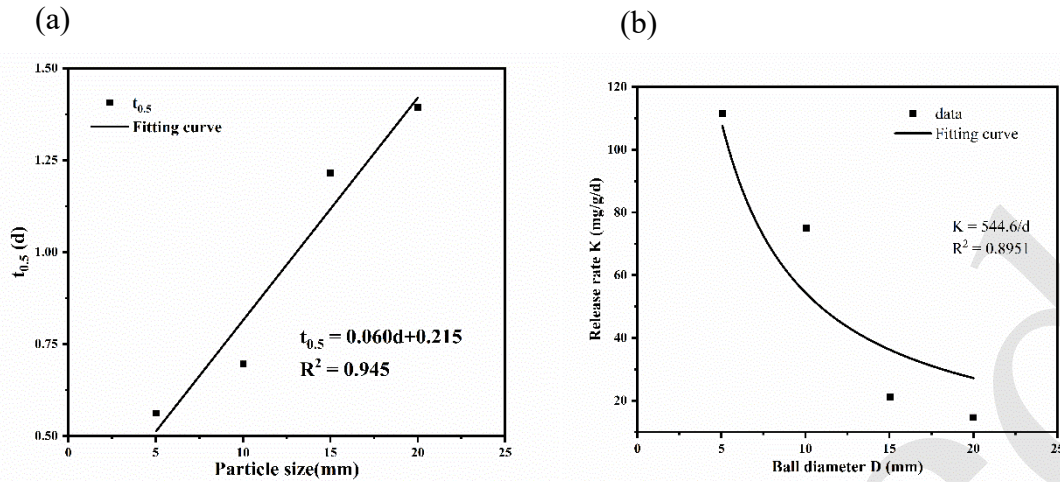


Fig. 14 Relationship and fitting curve between (a) half-life and particle size, (b) release rate and ball diameter

## 4 Discussion

### 4.1 Compatibility between PRB flow rate and PS release rate

Given 2500 20 mm sustained-release sodium persulfate balls in a PRB cross-section ( $A$ ), with  $M=8.85$  g each, the release rate ( $K$ ) is 23.63 mg/g/d, the released sodium persulfate is 522.81  $A$  g/d, which is able to oxidize COD 42.7 $A$  g/d. Given the concentration of COD of 200 mg/L, the maximum flow rate in the PRB is 0.21 m/d.

In order for an engineering PRB to work effectively, the appropriate amount of PS released should be consumed for COD oxidation. This requires that at a given time, sufficient PS ( $Q_{PS}$ ) is being released for oxidizing the cumulative quantity of COD ( $Q_{COD}$ ) in the permeation fluids. The latter  $Q_{COD}$  is quantified as  $A \cdot V_0 \cdot C_0 \cdot t$ , where  $A$  denotes the PRB water cross-section ( $m^2$ ),  $V_0$  denotes flow rate (m/d),  $C_0$  denotes the concentration of COD (mg/L), and  $t$  is time (d). The former ( $Q_{PS}$ ) is quantified as  $\frac{A}{D^2} \times 10^9 \cdot M \cdot K$ , where  $D$  represents ball diameter (mm) and  $M$  is the mass of the sustained-release ball (g per unit).

According to the batch test, the ratio of  $Q_{COD}$ :  $Q_{PS}$  is at equilibrium, namely:

$$aAV_0C_0 \leq \frac{A}{D^2MK} \times 10^6, \quad (13)$$

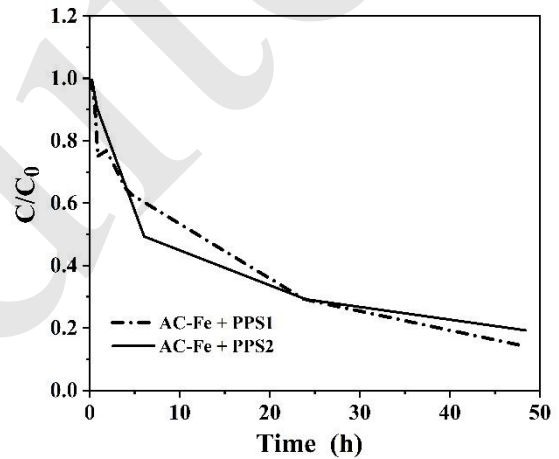


Fig. 15 Removal effect of COD with oxidizing filler (by using Fe(II)-loaded activated carbon with sustained-release sodium persulfate balls)

### 4.2 Compatibility of PS release rate and COD oxidation rates

In order to allow sufficient time for COD oxidation, the rate constant of COD consumption (oxidation) should be similar to the PS release rate. The kinetic chemical reaction results of Fe(II)-AC catalyzed sustained-release balls oxidizing COD (Fig. 16) can be fitted ( $R^2=0.9452$ ) by the 1<sup>st</sup>-order kinetic reaction:

$$R_{COD} = k \cdot \frac{\partial [COD]}{\partial t}, \quad (14)$$

where the half-life is 0.43 d, and the rate constant

$R_{\text{COD}}$  is  $0.08 \text{ h}^{-1}$ . The oxidation reaction half-life (0.43 d) is close to the PS release half-life of a 5 mm ball (0.56 d), which satisfies the compatibility condition (Fig. 16).

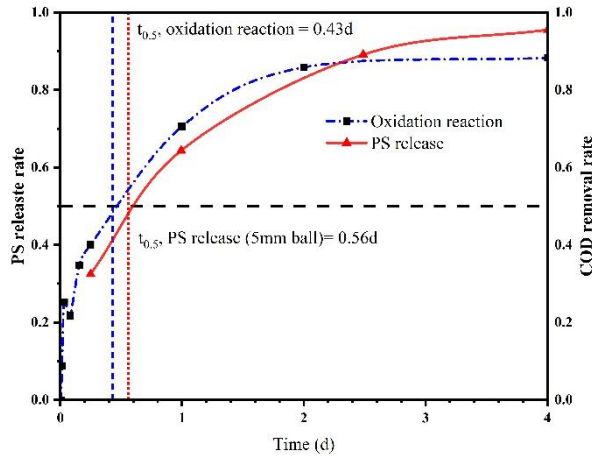


Fig. 16 Kinetic chemical reaction results of Fe-AC catalyzed sustained-release balls oxidizing COD.

### 4.3 Simulation of PRB Serviceability

The COD concentration from the effluent in the column test showed a removal rate higher than 80% in 40 hours. Using STANMOD-CXTFIT software, the retardation factor  $R_d$  and diffusion coefficient  $D_h$  were estimated to be 1.27 and  $15.6 \text{ cm}^2/\text{d}$ , respectively, based on the following equation:

$$\frac{C_f}{C_0} = \frac{1}{2} \operatorname{erfc}\left(\frac{R_d L - v_s t_b}{2\sqrt{D_h R_d t_b}}\right) + \frac{1}{2} \exp\left(\frac{v_s L}{D_h}\right) \operatorname{erfc}\left(\frac{R_d L + v_s t_b}{2\sqrt{D_h R_d t_b}}\right), \quad (15)$$

where  $C_f$  is the outflow concentration;  $C_0$  is the initial concentration;  $R_d$  is the blocking factor;  $L$  is the thickness of the seepage path;  $V_s$  is the flow rate of pore water;  $t_b$  is time;  $D_h$  is the hydrodynamic dispersion coefficient.

Given that  $V_0=0.21 \text{ m/d}$ ,  $R_d=1.27$ , and  $L=3 \text{ m}$  (thickness of PRB), the service life of this PRB with a breakthrough threshold of 10% is 2 years, which is of practical use.

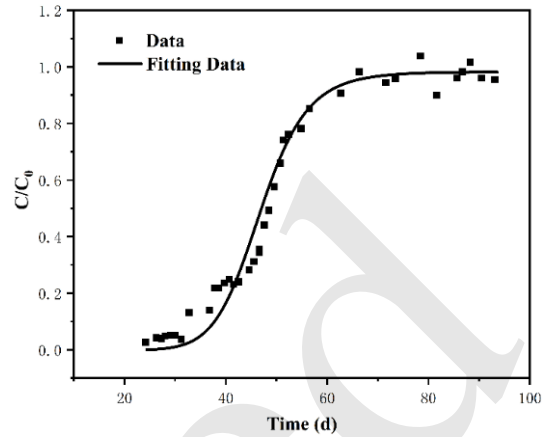


Fig. 17 Breakthrough curve of COD in a column test

## 5 Conclusions

The feasibility of sodium persulfate as a strong oxidant used in a permeable reactive barrier (PRB) was verified in terms of COD oxidation efficiency and rate of chemical kinetic reaction. Enhancement of the oxidation efficiency was achieved by Fe(II)-loaded AC, which helps evenly distribute Fe(II), a high-efficiency oxidant, in the PRB. From the test results, the feasibility of sodium persulfate used in PRB was demonstrated:

(1) The optimum dosage ratio of Fe-AC: sustained-release PS balls and PS: COD was obtained at first as 1:2 and 12.24:1, which yielded the highest COD removal rate of 95%;

(2) The release rate ( $R$ ) of sustained PS release balls was linearly proportional to the ball diameter ( $D$ ):  $R = 544.6/D$ . In addition, the COD oxidation rate ( $t_{0.5}=0.43 \text{ d}$ ) was compatible with the PS release rate of balls under 5 mm ( $t_{0.5}=0.56 \text{ d}$ ). This substantiated the compatibility of the release rate of sustained PS balls and the kinetic oxidation rate of COD.

(3) The COD removal by sodium persulfate catalyzed by Fe(II)-loaded AC followed first-order kinetics, with a rate constant ( $K$ ) of  $0.83 \text{ hr}^{-1}$  (i.e. a half-life = 0.83 hrs). Similarly, COD removal by four pebbles of sustained-release sodium persulfate balls catalyzed by Fe(II)-loaded AC, followed pseudo-first-order kinetics, with rate constant ( $K$ ) of  $0.15 \text{ hr}^{-1}$  (i.e. a half-life of 4.62 hrs), while might

due to the pores and cracks on the balls.

(4) In comparison with certain carbon-based new materials used in PRB for COD removal, the sustained-release sodium persulfate ball addresses the issue of high effectiveness of sodium persulfate, which, due to the blocking risk and fast reaction rate, might otherwise be unsuitable as a PRB filling material. Based on the kinetic parameters discussed earlier, it is evident that the sustained-release sodium persulfate ball, catalyzed by Fe-AC, exhibits high COD removal effectiveness.

### Acknowledgement

This research was financially supported by the Ministry of Science and Technology of China (Award No.: 2019YFC1805002, 2018YFC1802300), the National Natural Science Foundation of China (Award No.: 42177118, 51779219), and the Basic Science Center Program for Multiphase Evolution in Hypergravity of the National Natural Science Foundation of China (Award No.: 51988101). Financial support from the Overseas Expertise Introduction Center for Discipline Innovation (B18047) is also acknowledged. The authors would also like to acknowledge the MOE Key Laboratory of Soft Soils and Geoenvironmental Engineering.

### Conflict of interest

The authors declare that they have no conflict of interest.

### References

- Abdullah B, Ilyas S, Tahir D, 2018. Nanocomposites fe/activated carbon/pva for microwave absorber: Synthesis and characterization. *Journal of Nanomaterials*, 2018:1-6. <https://doi.org/10.1155/2018/9823263>
- Barroso-Bogeat A, Alexandre-Franco M, Fernández-González C, et al., 2019. Activated carbon surface chemistry: Changes upon impregnation with al(iii), fe(iii) and zn(ii)-metal oxide catalyst precursors from  $\text{no}_3^-$  aqueous solutions. *Arabian Journal of Chemistry*, 12(8):3963-3976. <https://doi.org/10.1016/j.arabjc.2016.02.018>
- Budania R, Dangayach S, 2023. A comprehensive review on permeable reactive barrier for the remediation of groundwater contamination. *J Environ Manage*, 332:117343. <https://doi.org/10.1016/j.jenvman.2023.117343>
- Chen F, Yang Y, Chang M, et al., 2013. Release performance and mechanism of the slow-released persulfate materials. *Research of Environmental Sciences*, 26:995-1000. <https://doi.org/10.13198/j.issn.1001-6929.2013.09.013>
- Cheng S, Zhang L, Xia H, et al., 2016. Ultrasound and microwave-assisted preparation of fe-activated carbon as an effective low-cost adsorbent for dyes wastewater treatment. *RSC Advances*, 6(82):78936-78946. <https://doi.org/10.1039/c6ra14082c>
- Clifton C, Huie R, 1989. Rate constants for hydrogen abstraction reactions of the sulfate radical,  $\text{so}_4^-$ . *Alcohols. International Journal of Chemical Kinetics*, 21:677-687. <https://doi.org/10.1002/kin.550210807>
- Das K, Kendall C, Isabelle M, et al., 2008. Ftir of touch imprint cytology: A novel tissue diagnostic technique. *J Photochem Photobiol B*, 92(3):160-164. <https://doi.org/10.1016/j.jphotobiol.2008.05.012>
- Dong B, Zhang R, Gan Y, et al., 2019a. Multiple methods for the identification of heavy metal sources in cropland soils from a resource-based region. *Sci Total Environ*, 651(Pt 2):3127-3138. <https://doi.org/10.1016/j.scitotenv.2018.10.130>
- Dong CD, Chen CW, Hung CM, 2019b. Persulfate activation with rice husk-based magnetic biochar for degrading paes in marine sediments. *Environ Sci Pollut Res Int*, 26(33):33781-33790. <https://doi.org/10.1007/s11356-018-2423-2>
- Dumont G, Robert T, Marck N, et al., 2017. Assessment of multiple geophysical techniques for the characterization of municipal waste deposit sites. *Journal of Applied Geophysics*, 145:74-83. <https://doi.org/10.1016/j.jappgeo.2017.07.013>
- Feng M, Qu R, Zhang X, et al., 2015. Degradation of flumequine in aqueous solution by persulfate activated with common methods and polyhydroquinone-coated magnetite/multi-walled carbon nanotubes catalysts. *Water Res*, 85:1-10. <https://doi.org/10.1016/j.watres.2015.08.011>
- Gong Y, Li D, Luo C, et al., 2017. Highly porous graphitic biomass carbon as advanced electrode materials for supercapacitors. *Green Chemistry*, 19(17):4132-4140. <https://doi.org/10.1039/c7gc01681f>
- Goyal H, Tyagi T, Mondal P, 2023. Life cycle analysis and economic evaluation of adsorptive removal of arsenic from groundwater using gac and gac-fe adsorbents. *Journal of Cleaner Production*, 429:139557. <https://doi.org/10.1016/j.jclepro.2023.139557>
- Guo X, 2013. Advanced treatment of papermaking wastewater by sulfate radical-based advanced oxidation process. Master's Degree, South China University of Technology, Guangdong, China,
- Han Z, Ma H, Shi G, et al., 2016. A review of groundwater contamination near municipal solid waste landfill sites in china. *Sci Total Environ*, 569-570:1255-1264. <https://doi.org/10.1016/j.scitotenv.2016.06.201>
- Hussain I, Li M, Zhang Y, et al., 2017. Insights into the mechanism of persulfate activation with nzvi/bc nanocomposite for the degradation of nonylphenol. *Chemical Engineering Journal*, 311:163-172. <https://doi.org/10.1016/j.cej.2016.11.085>
- Kalaruban M, Loganathan P, Nguyen TV, et al., 2019. Iron-

- impregnated granular activated carbon for arsenic removal: Application to practical column filters. *Journal of Environmental Management*, 239:235-243. <https://doi.org/10.1016/j.jenvman.2019.03.053>
- Kamaraj M, Srinivasan NR, Assefa G, et al., 2020. Facile development of sunlit zno nanoparticles-activated carbon hybrid from pernicious weed as an operative nano-adsorbent for removal of methylene blue and chromium from aqueous solution: Extended application in tannery industrial wastewater. *Environmental Technology & Innovation*, 17 <https://doi.org/10.1016/j.eti.2019.100540>
- Kang N, Hua I, Rao P, 2004. Production and characterization of encapsulated potassium permanganate for sustained release as an in situ oxidant. *Industrial & Engineering Chemistry Research*, 43(17):5187-5193. <https://doi.org/10.1021/ie0499097>
- Khursan SL, Semes'ko DG, Safiullin RL, 2006. Quantum-chemical modeling of the detachment of hydrogen atoms by the sulfate radical anion. *Russian Journal of Physical Chemistry*, 80(3):366-371. <https://doi.org/10.1134/s0036024406030113>
- Kosson DS, Sloop HaVD, Eighmy TT, 1996. An approach for estimation of contaminant release during utilization and disposal of municipal waste combustion residues. *Journal of Hazardous Materials*, 47(1/3):43-75. [https://doi.org/10.1016/0304-3894\(95\)00109-3](https://doi.org/10.1016/0304-3894(95)00109-3)
- Krishnan KA, Haridas A, 2008. Removal of phosphate from aqueous solutions and sewage using natural and surface modified coir pith. *Journal of Hazardous Materials*, 152(2):527-535. <https://doi.org/10.1016/j.jhazmat.2007.07.015>
- Lee ES, Schwartz FW, 2007. Characteristics and applications of controlled-release  $\text{kmno}_4$  for groundwater remediation. *Chemosphere*, 66(11):2058-2066. <https://doi.org/10.1016/j.chemosphere.2006.09.093>
- Lee ES, Gupta N, 2014. Development and characterization of colloidal silica-based slow-release permanganate gel (srp-g): Laboratory investigations. *Chemosphere*, 109:195-201. <https://doi.org/10.1016/j.chemosphere.2014.01.020>
- Lee Y-C, Li Y-F, Chen M-J, et al., 2020. Efficient decomposition of perfluorooctanoic acid by persulfate with iron-modified activated carbon. *Water Res*, 174:115618. <https://doi.org/10.1016/j.watres.2020.115618>
- Li H, 2018. Investigation of typical organics for activate persulfate degradation. China University of petroleum (Beijing),
- Li J, Yang Z-H, Xu H-Y, et al., 2016a. Electrochemical treatment of mature landfill leachate using  $\text{ti}/\text{ruo}_2\text{-iro}_2$  and al electrode: Optimization and mechanism. *RSC Advances*, 6(53):47509-47519. <https://doi.org/10.1039/c6ra05080h>
- Li Z, 2016. Cranular activated carbon supported iron as a heterogeneous persulfate catalyst for the pretreatment of mature landfill leachate. Master of Engineering, Donghua University, Shanghai, China,
- Li Z, Yang Q, Zhong Y, et al., 2016b. Granular activated carbon supported iron as a heterogeneous persulfate catalyst for the pretreatment of mature landfill leachate. *RSC Advances*, 6(2):987-994. <https://doi.org/10.1039/c5ra21781d>
- Liang SH, Kao CM, Kuo YC, et al., 2011. In situ oxidation of petroleum-hydrocarbon contaminated groundwater using passive isco system. *Water Res*, 45(8):2496-2506. <https://doi.org/10.1016/j.watres.2011.02.005>
- Lin CW, Wu CH, Tang CT, et al., 2012. Novel oxygen-releasing immobilized cell beads for bioremediation of btex-contaminated water. *Bioresour Technol*, 124:45-51. <https://doi.org/10.1016/j.biortech.2012.07.099>
- Ma H, Xu S, Zhang X, et al., 2023a. N-doped coal-based carbon membrane coupling peroxymonosulfate activation for bisphenol a degradation: The role of micro-carbon structure and nitrogen species. *Journal of Cleaner Production*, 423 <https://doi.org/10.1016/j.jclepro.2023.138713>
- Ma H, Zhang X, Feng G, et al., 2023b. Carbon nanotube membrane armed with confined iron for peroxymonosulfate activation towards efficient tetracycline removal. *Separation and Purification Technology*, 312 <https://doi.org/10.1016/j.seppur.2023.123319>
- Mehrabi N, Soleimani M, Yeganeh MM, et al., 2015. Parameter optimization for nitrate removal from water using activated carbon and composite of activated carbon and  $\text{fe}_2\text{o}_3$  nanoparticles. *RSC Advances*, 5(64):51470-51482. <https://doi.org/10.1039/c5ra03920g>
- Omoike AI, Harmon D, 2019. Slow-releasing permanganate ions from permanganate core-manganese oxide shell particles for the oxidative degradation of an algae odorant in water. *Chemosphere*, 223:391-398. <https://doi.org/10.1016/j.chemosphere.2019.02.036>
- P., Neta, V., et al., 1977. Rate constants and mechanism of reaction of sulfate radical anion with aromatic compounds. *Journal of the American Chemical Society*, <https://doi.org/10.1021/ja00443a030>
- Padmaja S, Alfassi ZB, Neta P, et al., 1993. Rate constants for reactions of  $\text{so}_4\cdot^-$  radicals in acetonitrile. *International Journal of Chemical Kinetics*, 25(3):193-198. <https://doi.org/10.1002/kin.550250307>
- Rauscher L, Sakulthaew C, Comfort S, 2012. Using slow-release permanganate candles to remediate pah-contaminated water. *J Hazard Mater*, 241-242:441-449. <https://doi.org/10.1016/j.jhazmat.2012.09.064>
- Ross C, Murdoch LC, Freedman DL, et al., 2005. Characteristics of potassium permanganate encapsulated in polymer. *Journal of Environmental Engineering*, 131(8):1203-1211. [https://doi.org/10.1061/\(ASCE\)0733-9372\(2005\)131:8\(1203\)](https://doi.org/10.1061/(ASCE)0733-9372(2005)131:8(1203))

- Sakulthaew C, Chokejaroenrat C, 2016. Oxidation of 17 $\beta$ -estradiol in water by slow-release permanganate candles. *Environmental Engineering Science*, 33(4):224-234. <https://doi.org/10.1089/ees.2015.0456>
- Singh R, Chakma S, Birke V, 2023. Performance of field-scale permeable reactive barriers: An overview on potentials and possible implications for in-situ groundwater remediation applications. *Science of the Total Environment*, 858:158838. <https://doi.org/10.1016/j.scitotenv.2022.158838>
- Song XL, Wang C, Liu MQ, et al., 2018. Advanced treatment of biologically treated coking wastewater by persulfate oxidation with magnetic activated carbon composite as a catalyst. *Water Science and Technology*, 77(7):1891-1898. <https://doi.org/10.2166/wst.2018.069>
- Tian W, Zhang H, Qian Z, et al., 2018. Bread-making synthesis of hierarchically co@c nanoarchitecture in heteroatom doped porous carbons for oxidative degradation of emerging contaminants. *Applied Catalysis B: Environmental*, 225:76-83. <https://doi.org/10.1016/j.apcatb.2017.11.056>
- Tsitonaki A, Petri B, Crimi M, et al., 2010. In situ chemical oxidation of contaminated soil and groundwater using persulfate: A review. *Critical Reviews in Environmental Science and Technology*, 40:55-91. <https://doi.org/10.1080/10643380802039303>
- Veerakumar P, Panneer Muthuselvam I, Hung C-T, et al., 2016. Biomass-derived activated carbon supported fe<sub>3</sub>o<sub>4</sub> nanoparticles as recyclable catalysts for reduction of nitroarenes. *ACS Sustainable Chemistry & Engineering*, 4(12):6772-6782. <https://doi.org/10.1021/acssuschemeng.6b01727>
- Wang B, Zhang Y, Gao C, et al., 2023. Developing novel persulfate pellets to remediate btexs-contaminated groundwater. *Journal of Water Process Engineering*, 52 <https://doi.org/10.1016/j.jwpe.2023.103505>
- Wang J, 2017. Study on treatment of refractory organic wastewater by persulfate activated by iron based sludge-derived biochar. Doctor, Huangzhong University of Science & Technology,
- Wang Z, Lu Y, Wu Z, et al., 2014. Study on the interference of persulfate in the process of cod determination and its elimination. *Industrial Water Treatment*, 34(8):78-81. [https://doi.org/10.11894/1005-829x.2014.34\(8\).078](https://doi.org/10.11894/1005-829x.2014.34(8).078)
- Xu X-Y, Zeng G-M, Peng Y-R, et al., 2012. Potassium persulfate promoted catalytic wet oxidation of fulvic acid as a model organic compound in landfill leachate with activated carbon. *Chemical Engineering Journal*, 200-202:25-31. <https://doi.org/10.1016/j.cej.2012.06.029>
- Yang J, 2016. Study on advanced treatment of landfill leachate by persulfate. Master Degree, China University of Geosciences (Beijing), Beijing, China,
- Yang S, Oostrom M, Truex MJ, et al., 2016. Injectable silica-permanganate gel as a slow-release mno<sub>4</sub><sup>-</sup> source for groundwater remediation: Rheological properties and release dynamics. *Environ Sci Process Impacts*, 18(2):256-264. <https://doi.org/10.1039/c5em00559k>
- Yao Y, Chen H, Qin J, et al., 2016. Iron encapsulated in boron and nitrogen codoped carbon nanotubes as synergistic catalysts for fenton-like reaction. *Water Res*, 101:281-291. <https://doi.org/10.1016/j.watres.2016.05.065>
- Ye J, Chen X, Chen C, et al., 2019. Emerging sustainable technologies for remediation of soils and groundwater in a municipal solid waste landfill site -- a review. *Chemosphere*, 227:681-702. <https://doi.org/10.1016/j.chemosphere.2019.04.053>
- Zeng X, Huang Y, Zhang Y, et al., 2017. Elimination of persulfate interference in determination of cod in organic wastewater. *Journal of Chongqing University*, 40(12):79-86. <https://doi.org/10.11835/j.issn.1000-582X.2017.12.010>
- Zhang L, Tu LY, Liang Y, et al., 2018. Coconut-based activated carbon fibers for efficient adsorption of various organic dyes. *RSC Adv*, 8(74):42280-42291. <https://doi.org/10.1039/c8ra08990f>
- Zhang X, Feng M, Qu R, et al., 2016. Catalytic degradation of diethyl phthalate in aqueous solution by persulfate activated with nano-scaled magnetic cufe<sub>2</sub>o<sub>4</sub>/mwcnts. *Chemical Engineering Journal*, 301:1-11. <https://doi.org/10.1016/j.cej.2016.04.096>
- Zhao J, Sun Y, Zhang Y, et al., 2021. Heterogeneous activation of persulfate by activated carbon supported iron for efficient amoxicillin degradation. *Environmental Technology & Innovation*, 21 <https://doi.org/10.1016/j.eti.2020.101259>
- Zhao J, Sun Y, Zhang BT, et al., 2023. Amoxicillin degradation in the heat, light, or heterogeneous catalyst activated persulfate systems: Comparison of kinetics, mechanisms and toxicities. *J Environ Manage*, 348:119386. <https://doi.org/10.1016/j.jenvman.2023.119386>